Dynamics of Two-Phase Dusty Fluid Flow Along a Wavy Surface

Article *in* International Journal of Nonlinear Sciences and Numerical Simulation · January 2016

DOI: 10.1515/ijnsns-2015-0044

CITATIONS
6

READS
303

4 authors:

Sadia Siddiqa
COMSATS University Islamabad
87 PUBLICATIONS **655** CITATIONS
SEE PROFILE

Muhammad Abrar
Capital University of Science & Technology
7 PUBLICATIONS **33** CITATIONS
SEE PROFILE

Anwar Hossain
University of Dhaka
204 PUBLICATIONS **4,376** CITATIONS
SEE PROFILE

M. Awais
COMSATS University Islamabad
85 PUBLICATIONS **1,653** CITATIONS
SEE PROFILE

Sadia Siddiqa, M. N. Abrar, M. A. Hossain and M. Awais*

Dynamics of Two-Phase Dusty Fluid Flow Along a Wavy Surface

DOI 10.1515/ijnsns-2015-0044
Received April 13, 2015; accepted June 6, 2016

Abstract: This article provides the computational results of laminar, boundary layer flow of a dilute gas-particle mixture over a semi-infinite vertical wavy surface. The governing parabolic partial differential equations are switched into another frame of reference by using primitive variable formulations (PVF). Two-point finite difference scheme is applied to acquire the unknown quantities of the carrier and the particle phase. The results are obtained for the cases: (i) water–metal mixture and (ii) air–metal mixture and are displayed in the form of wall shear stress, wall heat transfer, velocity profile, temperature profile, streamlines and isotherms for different emerging physical parameters. The solutions are compared, as well, with the available data in the literature. Quantitative comparison shows good compatibility between the present and the previous results. For the dusty fluid model it is found that the rate of heat transfer reduces considerably when the amplitude of the sinusoidal waveform increases from 0 to 0.5.

Keywords: natural convection, vertical wavy surface, two-phase, dusty fluid

PACS® (2010). 44.35.+c, 47.11.Bc, 47.15.Cb

1 Introduction

The study of the flow of fluids, with suspended particles, have received gradually more and more attention due to its practical applications in various problem of atmospheric, engineering and physiological fields. To mention a few, gas-particle flow phenomenon are significant in solid rocket exhaust nozzles, nuclear reactors with gas-solid feeds, ablation cooling, blast waves moving over the earth's surface, conveying of powdered materials, fluidized beds, environmental pollutants, petroleum industry, purification of crude oil, physiological flows and other technological fields (see [1]). Initially, Farbar and Morley [2] made an attempt in which experimental data was generated for heat transfer by adding alumina-silica catalyst with air and concluded that the heat transfer coefficient of the gas-solid mixture increases appreciably. Kazakevich and Kravipin [3] did an experimental study on the aerodynamic resistance of a dusty gas, flowing through a system of pipes and showed that the resistance is less than that of the clear gas. Saffman [4], further, introduced the basic theoretical model for the flow of dusty fluid of the above phenomenon. Saffman [4] supported the results of [3] and showed that the dust particles in any gas have much larger inertia than that of the equivalent volume of air which ultimately reduces viscosity. Vimala [5] studied the incompressible dusty gas bounded by two infinite flat plates executing simple harmonic oscillations in their own planes and calculated the unknown velocity components by using the Laplace transform. Further, the model of Saffman [4] was extended by Marble [6] in which the author studied the dynamics of gas containing small solid particles. However, Marble's analysis was not valid for the entire length of the plate. It was shown that for gas-particle flow systems, the particle cloud was governed by four similarity parameters; each of which has a simple physical significance. The flow over a solid object of a viscous gas containing spherical solid particles was considered by Singleton [7] in which the author treated the cases of i) compressible and ii) incompressible dusty gas boundary layer flow. Further, Michael and Miller [8] discussed the solutions for two problems induced by the motion of a dusty gas, which occupies the semi-infinite space above a rigid plane boundary. They obtained the solutions for the following two cases when the plane moves parallel to itself: (i) in simple harmonic motion and (ii) impulsively from rest with uniform velocity. The effect on the steady flow past a sphere of a uniform upstream distribution of dust particles having a small relaxation time has been considered by Michael [9]. Power series solution of a dusty fluid over a semi-infinite flat plate for the regimes: $x << 1$ and $x >> 1$ were obtained by Datta and Mishra [10] and found that physical quantities like drag coefficient on

***Corresponding author: M. Awais,** Department of Mathematics, COMSATS Institute of Information Technology, Kamra Road, Attock, Pakistan, E-mail: awais_mm@yahoo.com
Sadia Siddiqa, Department of Mathematics, COMSATS Institute of Information Technology, Kamra Road, Attock, Pakistan, E-mail: saadiasiddiqa@gmail.com
M. N. Abrar, Department of Mathematics, Capital University of Science and Technology, Islamabad Pakistan
M. A. Hossain, Department of Mathematics, University of Dhaka, Dhaka, Bangladesh

the plate increases with an increase in concentration parameter. Later, effect of pressure gradient on friction and heat transfer in a dusty boundary layer was investigated by Agranat [11] in which approximate analytical expressions for the local skin friction and heat transfer were obtained and tested in the case of an incompressible carrier phase. Recently Roopa et al. [12] made an attempt to study the effect of radiation on mixed convection boundary layer flow and heat transfer of a dusty fluid over a stretching vertical surface and obtained numerical solutions by using RKF-45 method. A more recent and detailed analysis for natural convection flow of a dusty fluid along a vertical surface has been considered by Siddiqa et al. [13]. The authors solved the coupled system of equations numerically through implicit finite difference method.

It is worthy to mention that all the above studies examined smooth surfaces only. Perhaps irregular surfaces are sometimes more important in industries due to their applications in solar collectors, condensers in refrigerators, cavity wall insulating systems, grain storage containers, and industrial heat radiators. These surfaces are successful in industries because they can encounter small as well as large scale heat transfer (see [14]). Distribution of heat transfer along a semi-infinite vertical wavy surface of Newtonian fluid was initially discussed by Yao [15]. Later on rough surfaces were well exploited under several different circumstances, as discussed in references [16–25].

In the present study, natural convection dusty fluid flow is investigated over a vertical heated wavy surface. Two phase problem has not been analyzed yet over a wavy surface in the literature. Coordinate transformations, known as primitive variable formulations, are employed to transform the boundary layer equations into parabolic partial differential equations, which are numerically integrated by using the implicit finite difference method. These numerical results are obtained for the practical situations like: (i) water–metal mixture and (ii) air–metal mixture. Numerical results are obtained with a view to disclose the quantitative response of various flow parameters on the components of carrier phase/particle phase velocity, carrier phase (or particle phase) temperature, wall shear stress and wall heat transfer.

2 Analysis

In the present analysis, both the fluid and the dust particle clouds are supposed to be static at the beginning along a semi-infinite heated vertical wavy surface. Initially, the system is having a uniform temperature, T_∞. Suddenly,

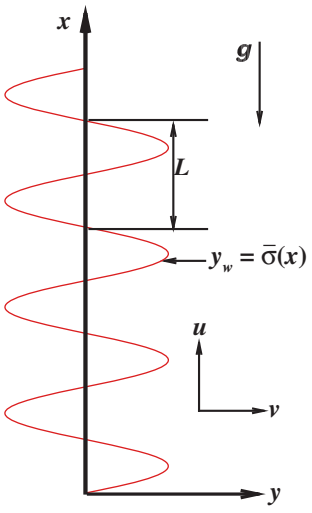

Figure 1: Physical model.

the wall $y = 0$ is heated to a temperature $T + \Delta T$ and natural convection starts due to this. It is assumed that x-axis is along the solid surface, whereas y-axis is in the direction normal to the surface as shown in Figure 1. All the fluid properties are considered constant except density, which obeys Boussinesq approximation and thus the density difference is indispensable to the natural convection motion and must be retained where they appear in the body force term (i. e., term multiplied by g, the acceleration due to gravity), but elsewhere the density variation is considered to be small enough and is to be neglected. Our detailed numerical work will assume that the surface exhibit sinusoidal deformations. The shape of the wavy surface is supposed to obey the following pattern:

$$y_w = \bar{\sigma}(x) = \bar{\alpha} \sin\left(\frac{2\pi x}{L}\right) \tag{1}$$

where L is the characteristic length scale associated with the wavy surface and $\bar{\alpha}$ the amplitude of wavy surface. Within the framework of the assumptions given in Siddiqa et al. [13], the governing boundary layer equations pertinent to the problem are given by (see [4, 13]):

For the gas phase:

$$\frac{\partial u}{\partial x} + \frac{\partial v}{\partial y} = 0 \tag{2}$$

$$\rho\left(u\frac{\partial u}{\partial x} + v\frac{\partial u}{\partial y}\right) = -\frac{\partial p}{\partial x} + \mu\left(\frac{\partial^2 u}{\partial x^2} + \frac{\partial^2 u}{\partial y^2}\right) + \rho g\beta(T - T_\infty) + \frac{\rho_p}{\tau_m}(u_p - u) \tag{3}$$

$$\rho\left(u\frac{\partial v}{\partial x} + v\frac{\partial v}{\partial y}\right) = -\frac{\partial p}{\partial y} + \mu\left(\frac{\partial^2 v}{\partial x^2} + \frac{\partial^2 v}{\partial y^2}\right) + \frac{\rho_p}{\tau_m}(v_p - v) \tag{4}$$

$$\rho c_p\left(u\frac{\partial T}{\partial x}+v\frac{\partial T}{\partial y}\right)=\kappa\left(\frac{\partial^2 T}{\partial x^2}+\frac{\partial^2 T}{\partial y^2}\right)+\frac{\rho_p c_s}{\tau_T}\left(T_p-T\right) \tag{5}$$

For the particle phase:

$$\frac{\partial u_p}{\partial x}+\frac{\partial v_p}{\partial y}=0 \tag{6}$$

$$\rho_p\left(u_p\frac{\partial u_p}{\partial x}+v_p\frac{\partial u_p}{\partial y}\right)=-\frac{\partial p_p}{\partial x}-\frac{\rho_p}{\tau_m}(u_p-u) \tag{7}$$

$$\rho_p\left(u_p\frac{\partial v_p}{\partial x}+v_p\frac{\partial v_p}{\partial y}\right)=-\frac{\partial p_p}{\partial y}-\frac{\rho_p}{\tau_m}(v_p-v) \tag{8}$$

$$\rho_p c_s\left(u_p\frac{\partial T_p}{\partial x}+v_p\frac{\partial T_p}{\partial y}\right)=-\frac{\rho_p c_s}{\tau_T}(T_p-T) \tag{9}$$

In the above system of equations $\mathbf{u}=(u,v)$, T, p, ρ, c_p, κ, μ, g and β are respectively the velocity vector in the (x,y) direction, temperature, pressure, density, specific heat at constant pressure, thermal conductivity, coefficient of viscosity of the fluid, acceleration due to gravity and volumetric coefficient of thermal expansion. Similarly, $\mathbf{u_p}=(u_p,v_p)$, T_p, p_p, ρ_p and c_s corresponds to the velocity vector, temperature, pressure, density and specific heat for the particle phase. In addition, τ_m is the relaxation time during which the velocity of the particle phase relative to the fluid is reduced to $1/e$ times its initial value and τ_T is the thermal relaxation time of particle phase during which the temperature of the particle phase relative to the fluid is $1/e$ times the initial value.

The fundamental equations stated above are to be solved under appropriate boundary conditions to determine the flow fields of the fluid and the dust particles. Therefore, boundary conditions are:

For the gas phase:

$$\begin{aligned}&u(x,y_w)=v(x,y_w)=T(x,y_w)-T_w=0\\&u(x,\infty)=T(x,\infty)-T_\infty=0\end{aligned} \tag{10}$$

For the particle phase:

$$\begin{aligned}&u_p(x,0)=v_p(x,0)=T_p(x,0)-T_w=0\\&u_p(x,\infty)=T_p(x,\infty)-T_\infty=0\end{aligned} \tag{11}$$

Following dependent and independent flow variables are chosen to make the system dimensionless:

$$\begin{gathered}u=\frac{\nu}{L}Gr^{1/2}U,\quad u_p=\frac{\nu}{L}Gr^{1/2}U_p,\quad v-\sigma_X u=\frac{\nu}{L}Gr^{1/4}V,\\ v_p-\sigma_X u_p=\frac{\nu}{L}Gr^{1/4}V_p,\quad \Theta=\frac{T-T_\infty}{T_w-T_\infty},\quad \Theta_p=\frac{T_p-T_\infty}{T_w-T_\infty},\\ p=\frac{\rho\nu^2 Gr}{L}P,\quad p_p=\frac{\rho\nu^2 Gr}{L}P_p,\quad X=\frac{x}{L},Y=\frac{y-\sigma_X}{L}Gr^{1/4},\\ Gr=\frac{g\beta(T_w-T_\infty)L^3}{\nu^2},\quad \sigma=\frac{\bar\sigma}{L},\quad \alpha=\frac{\bar\alpha}{L},\quad \sigma_x=\frac{d\bar\sigma}{dx}=\frac{d\sigma}{dX}\end{gathered} \tag{12}$$

System of eqs (2)–(11) becomes:

$$\frac{\partial U}{\partial X}+\frac{\partial V}{\partial Y}=0 \tag{13}$$

$$\begin{aligned}U\frac{\partial U}{\partial X}+V\frac{\partial U}{\partial Y}=&-\frac{\partial P}{\partial X}+\sigma_X Gr^{1/4}\frac{\partial P}{\partial Y}+\left(1+\sigma_X^2\right)\frac{\partial^2 U}{\partial Y^2}\\&+\Theta-D_\rho\alpha_d(U-U_p)\end{aligned} \tag{14}$$

$$\begin{aligned}\sigma_X\left(U\frac{\partial U}{\partial X}+V\frac{\partial U}{\partial Y}\right)+\sigma_{XX}U^2=&-Gr^{1/4}\frac{\partial P}{\partial Y}+\sigma_X\left(1+\sigma_X^2\right)\frac{\partial^2 U}{\partial Y^2}\\&-D_\rho\alpha_d\sigma_X(U-U_p)\end{aligned} \tag{15}$$

$$U\frac{\partial\Theta}{\partial X}+V\frac{\partial\Theta}{\partial Y}=\frac{1}{\mathrm{Pr}}\left(1+\sigma_X^2\right)\frac{\partial^2\Theta}{\partial Y^2}-\frac{2}{3\mathrm{Pr}}D_\rho\alpha_d\left(\Theta-\Theta_p\right) \tag{16}$$

$$\frac{\partial U_p}{\partial X}+\frac{\partial V_p}{\partial Y}=0 \tag{17}$$

$$U_p\frac{\partial U_p}{\partial X}+V_p\frac{\partial U_p}{\partial Y}=-\frac{\partial P_p}{\partial X}+\sigma_X Gr^{1/4}\frac{\partial P_p}{\partial Y}-\alpha_d(U_p-U) \tag{18}$$

$$\sigma_X\left(U_p\frac{\partial U_p}{\partial X}+V_p\frac{\partial U_p}{\partial Y}\right)+\sigma_{XX}U_p^2=-Gr^{1/4}\frac{\partial P_p}{\partial Y}-\alpha_d\sigma_X(U_p-U) \tag{19}$$

$$U_p\frac{\partial\Theta_p}{\partial X}+V_p\frac{\partial\Theta_p}{\partial Y}=-\frac{2\alpha_d}{3\gamma\mathrm{Pr}}\left(\Theta_p-\Theta\right) \tag{20}$$

The boundary conditions for the gas phase becomes:

$$\begin{aligned}&U(X,0)=V(X,0)=\Theta(X,0)-1=0\\&U(X,\infty)=\Theta(X,\infty)=0\end{aligned} \tag{21}$$

Similarly, for the particle phase boundary conditions are:

$$\begin{aligned}&U_p(X,0)=V_p(X,0)=\Theta_p(X,0)-1=0\\&U_p(X,\infty)=\Theta_p(X,\infty)=0\end{aligned} \tag{22}$$

where $\sigma(X)=\alpha sin(2\pi X)$. Numerical solutions will be obtained for this particular form of σ, later. For other shapes of the surface, a similar computation can be carried out by simply inputting the appropriate function for σ. Further, the interaction terms between the gas and the particles are expressed as follows:

- $\gamma(=c_s/c_p)$ is the specific heat ratio of mixture. For different gas-particle combinations, γ may vary between 0.1 and 10.0, and in such cases, either the temperature or the velocity tends to reach equilibrium faster (see Rudinger [1]).
- $D_\rho(=\rho_p/\rho)$ is the mass concentration of particle phase or the ratio of densities of the fluid and the dust particles.
- $\mathrm{Pr}(=\kappa/\rho c_p\nu)$ is the gas Prandtl number.

- $\tau_T = 1.5\gamma\tau_m \mathrm{Pr}$ is the relation between thermal relaxation time (τ_T) and velocity relaxation time (τ_m); indicating that τ_T is obeying the Stokes law. In the context of droplet or particle laden gas flows, these are commonly assumed forms for the velocity and temperature relaxation processes (see Marble [6]).
- $\alpha_d = L^2/\nu\tau_m Gr^{1/2}$ is the dust parameter depending on the relaxation time of the particles and the buoyancy force. It can be observed that for $\alpha_d = 0$ the flow governs by the natural convection in the absence of the dust particles.

It is worthy to mention that eqs (15) and (19) respectively indicate that the pressure gradient of the gas and the particle phase along the Y direction are of $O(Gr^{-1/4})$, which implies that the lowest order pressure gradient of both phases along the X direction can be determined from the inviscid-flow solution. In the present problem, this pressure gradient is zero because there is no externally induced free stream. Equation (15) further shows that $Gr^{1/4}\partial P/\partial Y$ is of $O(1)$ and is determined by the left-hand side of this equation. Thus, the elimination of $\partial P/\partial Y$ from eqs (14) and (15) leads to:

$$U\frac{\partial U}{\partial X} + V\frac{\partial U}{\partial Y} = (1+\sigma_X^2)\frac{\partial^2 U}{\partial Y^2} - \frac{\sigma_X\sigma_{XX}}{1+\sigma_X^2}U^2 + \frac{1}{1+\sigma_X^2}\Theta - D_\rho\alpha_d(U-U_p) \tag{23}$$

On the similar lines, eq. (19) depicts that $Gr^{1/4}\partial P_p/\partial Y$ is of $O(1)$. Therefore, removal of $\partial P_p/\partial Y$ from eqs (18) and (19) results into:

$$U_p\frac{\partial U_p}{\partial X} + V_p\frac{\partial U_p}{\partial Y} = -\frac{\sigma_X\sigma_{XX}}{1+\sigma_X^2}U_p^2 - \alpha_d(U_p - U) \tag{24}$$

To establish the solutions of the coupled equations (13), (16), (17), (20), (23), (24) along with the boundary conditions (21)–(22), we switch into another system of equations with the help of primitive variable formulations.

3 Primitive variable formulation (PVF)

Before applying the numerical scheme, following set of continuous transformations are introduced:

$$\begin{aligned} &U = X^{\frac{1+n}{2}}\ \bar{U}(\bar{X},\bar{Y}), U_p = X^{\frac{1+n}{2}}\bar{U}_p(\bar{X},\bar{Y}), V = X^{-\frac{1-n}{4}}\bar{V}(\bar{X},\bar{Y}),\\ &V_p = X^{-\frac{1-n}{4}}\bar{V}_p(\bar{X},\bar{Y}), \Theta = X^n\bar{\Theta}(\bar{X},\bar{Y}),\\ &\Theta_p = X^n\bar{\Theta}_p(\bar{X},\bar{Y}), Y = X^{\frac{1-n}{4}}\bar{Y}, X = \bar{X} \end{aligned} \tag{25}$$

Introducing eq. (25) into eqs (13), (16), (17), (20), (23), (24) along with the boundary conditions (21)–(22), one gets:

$$\frac{1+n}{2}\bar{U} + \bar{X}\frac{\partial\bar{U}}{\partial\bar{X}} - \frac{1-n}{4}\bar{Y}\frac{\partial\bar{U}}{\partial\bar{Y}} + \frac{\partial\bar{V}}{\partial\bar{Y}} = 0 \tag{26}$$

$$\frac{1+n}{2}\bar{U}^2 + \bar{X}\bar{U}\frac{\partial\bar{U}}{\partial\bar{X}} + \left(\bar{V} - \frac{1-n}{4}\bar{Y}\bar{U}\right)\frac{\partial\bar{U}}{\partial\bar{Y}} = (1+\sigma_{\bar{X}}^2)\frac{\partial^2\bar{U}}{\partial\bar{Y}^2} + \frac{\bar{\Theta}}{(1+\sigma_{\bar{X}}^2)} - \frac{\sigma_{\bar{X}}\sigma_{\bar{X}\bar{X}}}{1+\sigma_{\bar{X}}^2}\bar{X}\bar{U}^2 - D_\rho\alpha_d\bar{X}^{\frac{1-n}{2}}(\bar{U}-\bar{U}_p) \tag{27}$$

$$n\bar{U}\bar{\Theta} + \bar{X}\bar{U}\frac{\partial\bar{\Theta}}{\partial\bar{X}} + \left(\bar{V} - \frac{1-n}{4}\bar{Y}\bar{U}\right)\frac{\partial\bar{\Theta}}{\partial\bar{Y}} = \frac{1}{\mathrm{Pr}}(1+\sigma_{\bar{X}}^2)\frac{\partial^2\bar{\Theta}}{\partial\bar{Y}^2} - \frac{2}{3\mathrm{Pr}}D_\rho\alpha_d\bar{X}^{\frac{1-n}{2}}(\bar{\Theta}-\bar{\Theta}_p) \tag{28}$$

$$\frac{1+n}{2}\bar{U}_p + \bar{X}\frac{\partial\bar{U}_p}{\partial\bar{X}} - \frac{1-n}{4}\bar{Y}\frac{\partial\bar{U}_p}{\partial\bar{Y}} + \frac{\partial\bar{V}_p}{\partial\bar{Y}} = 0 \tag{29}$$

$$\frac{1+n}{2}\bar{U}_p^2 + \bar{X}\bar{U}_p\frac{\partial\bar{U}_p}{\partial\bar{X}} + \left(\bar{V}_p - \frac{1-n}{4}\bar{Y}\bar{U}_p\right)\frac{\partial\bar{U}_P}{\partial\bar{Y}} = -\frac{\sigma_{\bar{X}}\sigma_{\bar{X}\bar{X}}}{1+\sigma_{\bar{X}}^2}\bar{X}\bar{U}_p^2 - \alpha_d\bar{X}^{\frac{1-n}{2}}(\bar{U}_p - \bar{U}) \tag{30}$$

$$n\bar{U}_p\bar{\Theta}_p + \bar{X}\bar{U}_p\frac{\partial\bar{\Theta}_p}{\partial\bar{X}} + \left(\bar{V}_p - \frac{1-n}{4}\bar{Y}\bar{U}_p\right)\frac{\partial\bar{\Theta}_p}{\partial\bar{Y}} = -\frac{2\alpha_d}{3\gamma\mathrm{Pr}}\bar{X}^{\frac{1-n}{2}}(\bar{\Theta}_p - \bar{\Theta}) \tag{31}$$

The boundary conditions are:

$$\begin{aligned} &\bar{U}(\bar{X},0) = \bar{U}_p(\bar{X},0) = \bar{V}(\bar{X},0) = \bar{V}_p(\bar{X},0) = \bar{\Theta}(\bar{X},0) - 1\\ &\quad = \bar{\Theta}_p(\bar{X},0) - 1 = 0\\ &\bar{U}(\bar{X},\infty) = \bar{U}_p(\bar{X},\infty) = \bar{\Theta}(\bar{X},0) = \bar{\Theta}_p(\bar{X},\infty) = 0 \end{aligned} \tag{32}$$

The system (26)–(32) forms a complex set of equations which brings up two special cases. That is, for the pure vertical surface (when $\alpha = 0.0$), the model comes up with the solutions of Siddiqa et al. [13]. In addition to this, if dust parameter (α_d) or mass concentration parameter (D_ρ) is ignored then the current problem retrieves the results of Yao [15], provided the power index n is set to be 0. Comparison with both these studies is done in the later section. The set of partial differential equations (26)–(32) are solved numerically for various range of the parameters like: γ, D_ρ, α_d and α.

4 Solution methodology

The continuity, momentum and energy equations of carrier and disperse phase, given in eqs (26) to (31)

subject to the boundary conditions (32), are solved numerically with the aid of the implicit finite difference method, which implies Thomas algorithm as a solver. Since the equations are parabolic in $\bar{X}$, therefore solutions can be marched in the downstream direction. The computational domain is discretized over the entire boundary layer region. Keeping numerical stability in view, two-point central difference and backward difference quotients are respectively used for diffusion and convective terms. The resulting system of algebraic equations can be cast into a tri-diagonal matrix equation, which is solved via Thomas algorithm. This algorithm works on the following pattern:

1. Set the suitable initial and boundary conditions.
2. Solve the unknowns $\bar{U}, \bar{U}_p, \bar{\Theta}, \bar{\Theta}_p$ at $\bar{Y}=0$. It means that these unknowns satisfy the convergence criteria.
3. Solve for the next step $\bar{Y}_j = \bar{Y}_{j-1} + \Delta\bar{Y}$ by using the solution position.
4. The computations are iterated until the unknown quantities meet the convergence criteria at the streamwise position. The convergence criteria is:
5. Repeat steps 2–4 for $\bar{X}$ maximum.

$$\max|\bar{U}_{i,j}| + \max|\bar{U}_{p_{i,j}}| + \max|\bar{V}_{i,j}| + \max|\bar{V}_{p_{i,j}}| + \max|\bar{\Theta}_{i,j}| + \max|\bar{\Theta}_{p_{i,j}}| \le 10^{-5}$$

In the computation procedure, continuity equation of the carrier and the particle phase are used to obtain normal velocity component $\bar{V}$ and $\bar{V}_p$ respectively by using the following discretization:

$$\bar{V}_{i,j} = \bar{V}_{i-1,j} + \left(\frac{1-n}{4}\bar{Y}\left(\bar{U}_{i,j} - \bar{U}_{i-1,j}\right) - \frac{1+n}{2}\Delta\bar{Y}\bar{U}_{i,j} - \frac{1-n}{2}\frac{\bar{X}\Delta\bar{Y}}{\Delta\bar{X}}\left(\bar{U}_{i,j} - \bar{U}_{i,j-1} + \bar{U}_{i-1,j} - \bar{U}_{i-1,j-1}\right)\right) \tag{33}$$

and

$$\bar{V}_{p_{i,j}} = \bar{V}_{p_{i-1,j}} + \left(\frac{1-n}{4}\bar{Y}\left(\bar{U}_{p_{i,j}} - \bar{U}_{p_{i-1,j}}\right) - \frac{1+n}{2}\Delta\bar{Y}\bar{U}_{p_{i,j}} - \frac{1-n}{2}\frac{\bar{X}\Delta\bar{Y}}{\Delta\bar{X}}\left(\bar{U}_{p_{i,j}} - \bar{U}_{p_{i,j-1}} + \bar{U}_{p_{i-1,j}} - \bar{U}_{p_{i-1,j-1}}\right)\right) \tag{34}$$

At present, rectangular computational domain is used with grid point distribution at equal spacing. In the normal direction ($\bar{Y}$), 1501 uniform grid points are employed. Additionally, there are 1001 grid points in the marching direction. In the program test, a finer axial step size, $\Delta\bar{X} = \bar{X}_i - \bar{X}_{i-1} = 0.01$, is found to give acceptable accuracy. The computation has been started from $\bar{X}_i = 0.0$ and then marched up to $\bar{X}_i = 10.0$ by taking uniform grids. By comparing the results for different grid size in $\bar{Y}$ directions, we reached at the conclusion to choose $\Delta\bar{Y} = 0.03$ and the value of the boundary layer $\bar{Y}_\infty$ is 50.0, which actually corresponds to the condition $\bar{Y} \to \infty$ and it lies very well outside the momentum and thermal boundary layers of the corresponding phase. In the numerical procedure the iterative scheme operates along with an under relaxation coefficient, which allows a much faster convergence rate while solving the set of coupled nonlinear equations and typically it lies between 0 and 1. In our work this coefficient is taken to be 0.5.

It is significant to investigate the behavior of the dimensionless ratios employed in heat transfer calculations. For this, coefficient of Nusselt number, Q_w, is required to compute and it can be calculated from the following relation:

$$Q_w = NuGr^{-1/4}\bar{X}^{\frac{1-n}{4}} = -\left(1+\sigma_{\bar{X}}^2\right)^{1/2}\left(\frac{\partial\bar{\Theta}}{\partial\bar{Y}}\right)_{\bar{Y}=0} \tag{35}$$

Now the numerical results obtained for the key parameters are discussed in the section below.

5 Numerical results

At present a two phase dusty fluid model with effective gas properties is constituted. The complete set of governing equations for the two phase model (26)-(32) are solved numerically from implicit finite difference scheme. In order to gain some understanding of this dusty fluid problem over the vertical wavy surface, numerical results are examined in terms of heat transfer rate, velocity and temperature profiles, and streamlines and isotherms for several important parameters. The point of interest is the calculation of heat transfer rate under the dominant influence of mass concentration parameter, D_ρ, specific heat ratio parameter, γ, amplitude of the wavy surface, α, dust parameter, α_d against the crosswise coordinate $\bar{X}$. In order to find the optimal grid size, different values of $\Delta\bar{Y}$ are tested. The graphs are plotted for a range of various $\Delta\bar{Y}$ (0.005, 0.05, 0.1, 0.25, 0.5) in Figure 2 and it is observed

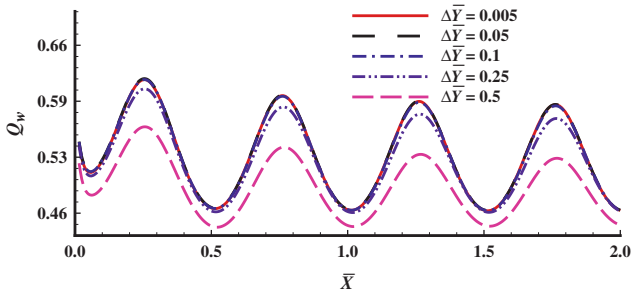

Figure 2: Grid independent test by taking $\Delta\bar{Y} = 0.005, 0.05, 0.1, 0.25, 0.5$ while $\mathrm{Pr} = 0.7$, $n = 0.0$, $D_\rho = 10.0$, $\alpha_d = 1.0$, $\alpha = 0.1$ and $\gamma = 0.45$.

that the optimal value for which solutions become independent of grid size is $\Delta\bar{Y} \le 0.1$. In this paper, some practical examples: i) metal particles in air ($D_\rho = 10^4$, Pr = 0.7, $\gamma = 0.45$) and ii) metal particles in water ($D_\rho = 10.0$, Pr = 7.0, $\gamma = 0.1$) are taken into consideration for computation purpose (see Apazidis [26]).

It should be noted that the numerical results obtained herein, reduce to those reported by Yao [15] provided the dusty parameter (α_d) and the power index, n, are zero. These results are presented in Figure 3 which shows quite an excellent agreement between the two studies. This comparison also validates our present numerical scheme. Besides this, solutions are also compared with one of the recent study of Siddiqa et al. [13] for flat plate problem. These results are retrieved for $n = 0.0, 1.0$, $D_\rho = 0.0, 5.0$, Pr = 0.005, $\gamma = 1.0$, $\alpha_d = 1.0$, $\alpha = 0.0$ and presented in Table 1. In [13], the authors introduced axial coordinate as: $\xi = \alpha_d \bar{X}^{\frac{1-n}{2}}$, but in our formulation this scaling is not used. Therefore, this comparison can be done if we re-scale our axial coordinate to make the model compatible. After that, results are obtained for the parameters (γ, D_ρ, α_d and α) and the computational values, again show good comparison between the studies.

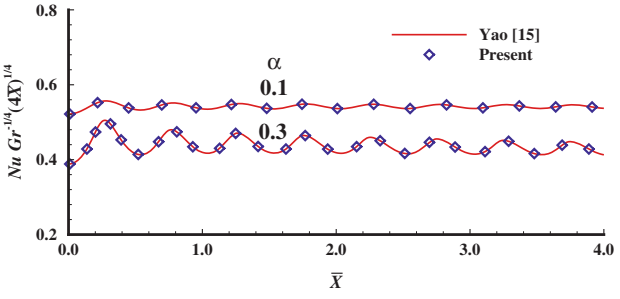

Figure 3: Local Nusselt number coefficient for $\alpha = 0.1, 0.3$ while Pr = 1.0, $D_\rho = 0.0$, $\alpha_d = 0.0$ and $\gamma = 1.0$.

Table 2: Numerical values of Q_w for $n = 0.0, 1.0$, $D_\rho = 0.2$, Pr = 5.0, $\alpha_d = 0.5$, $\gamma = 0.1$ and $\alpha = 0.25$.

$\bar{X}$	Q_w	
	$n = 0.0$	$n = 1.0$
0.01999	0.49564	0.71781
0.5095	0.51459	0.72958
0.009	0.51401	0.73599
0.008	0.51047	0.74038
0.007	0.50573	0.74118
0.006	0.50050	0.74051
0.005	0.49507	0.73904
0.004	0.48955	0.73707
0.003	0.48402	0.73478
0.002	0.47853	0.73225
0.001	0.47310	0.72955
0.0	0.46774	0.72672

Further, the numerical values of Q_w for $n = 0.0, 1.0$, $D_\rho = 0.2$, Pr = 5.0, $\alpha_d = 0.5$, $\gamma = 0.1$ and $\alpha = 0.25$ are entered in Table 2. These values indicate that heat flux rate increases due to the increment in the power index n. Therefore, n has distinctive role and can be served to enhance the heat transfer rate. Rest of the results are obtained for $n = 0.0$ only.

The characteristic distribution of the parameter $\gamma (= 0.1, 0.45)$ in the boundary layer for Pr = 0.7, 7.0, $D_\rho = 10.0, 10,000.0$, $\alpha_d = 0.5$ and $\alpha = 0.3$ is given in Figure 4. This shows, in effect, a gradual increase in the rate of heat transfer for increasing values of γ. Interestingly $\gamma = 0.1$ reflects that the specific heat of the gas at constant pressure is less than that of the specific heat of the particle phase, i. e., $c_s < c_p$. It can be noted that low specific heat ratio causes a relatively small increase in temperature gradient as compared to large γ. Therefore, γ establishes the relationship between the fluid and the

Table 1: Numerical values of Q_w for $n = 0.0, 1.0$, $D_\rho = 0.0, 5.0$, Pr = 0.005, $\gamma = 1.0$, $\alpha_d = 1.0$, $\alpha = 0.0$.

$\bar{X}$	Q_w							
	$n = 0.0$				$n = 1.0$			
	$D_\rho = 0.0$		$D_\rho = 5.0$		$D_\rho = 0.0$		$D_\rho = 5.0$	
	Present	Siddiqa et al. [13]	Present	Siddiqa et al. [13]	Present	Siddiqa et al. [13]	Present	Siddiqa et al. [13]
1.0	0.04169	0.04170	0.06397	0.06391	0.06691	0.06689	0.10345	0.10355
2.0	0.04169	0.04170	0.06399	0.06398	0.06691	0.06689	0.10369	0.10409
4.0	0.04169	0.04170	0.06401	0.06401	0.06691	0.06689	0.10401	0.10436
6.0	0.04169	0.04170	0.06401	0.06402	0.06691	0.06689	0.10433	0.10440
7.0	0.04169	0.04170	0.06401	0.06402	0.06691	0.06689	0.10441	0.10442
8.0	0.04169	0.04170	0.06401	0.06402	0.06691	0.06689	0.10442	0.10443
9.0	0.04169	0.04170	0.06401	0.06402	0.06691	0.06689	0.10443	0.10444
10.0	0.04169	0.04170	0.06401	0.06402	0.06691	0.06689	0.10445	0.10445

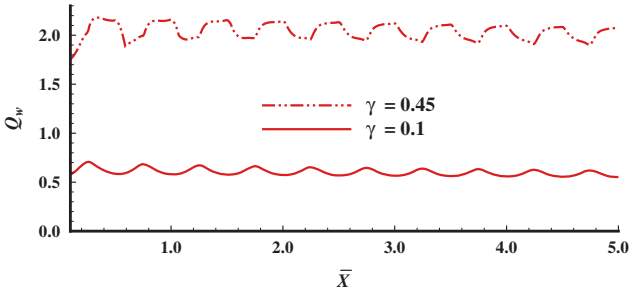

Figure 4: Local Nusselt number coefficient for $\gamma = 0.45$(air), 0.1 (water), Pr = 0.7(air), 7.0(water), $D_\rho = 10{,}000.0$(air), 10.0(water) while $\alpha_d = 0.5$ and $\alpha = 0.3$.

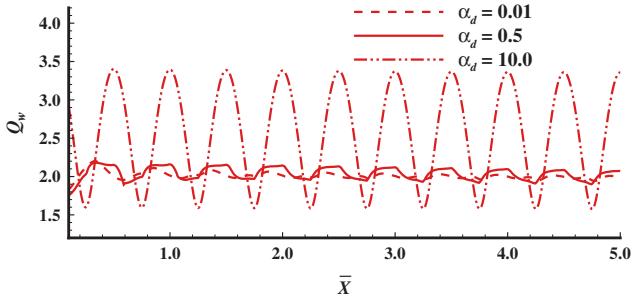

Figure 6: Local Nusselt number coefficient for $\alpha_d = 0.01, 0.5, 10.0$, Pr = 0.7, $D_\rho = 10, 000.0$, $\alpha = 0.3$ and $\gamma = 0.45$.

particle phase, which in principle, predicts the magnitude of temperature change that are essential skills in working with energy and chemical systems.

The numerical values of Q_w for some values of amplitude of the wavy surface parameter, α, is presented through Figure 5. The results for $\alpha = 0.0$ are those which are valid for the purely vertical plate problem. Therefore, for $\alpha = 0.0$ the waviness of the surface disappears and the numerical values show the solution of natural convection dusty fluid over a smooth plate. As a whole the rate of heat transfer reduces when the amplitude of the sinusoidal waveform increases. As the amplitude increases the shape of the wave gradually changes from sinusoidal waveform to the unusual shape. The reduction in the magnitude of the temperature gradient happened due to the simultaneous influence of (1) centrifugal force and (2) buoyancy force. Highest steeper peak points are found near the vicinity of the wavy surface. The results encourage us to conclude that velocity of the fluid increases, which ultimately lower down the magnitude of Q_w. Therefore, the current analysis declares clear reduction in the quantity Q_w.

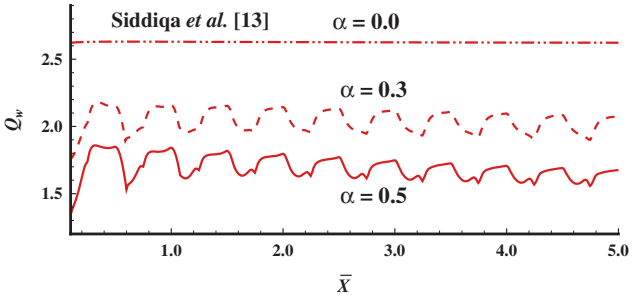

Figure 5: Local Nusselt number coefficient for air–metal mixture with $\alpha = 0.0, 0.3, 0.5$, Pr = 0.7, $D_\rho = 10, 000.0$, $\alpha_d = 0.5$ and $\gamma = 0.45$.

Variation of dust parameter is analyzed in Figure 6 by setting: $\alpha_d = 0.01, 0.5, 10.0$, Pr = 0.7, $D_\rho = 10000.0$, $\alpha = 0.3$ and $\gamma = 0.45$. It is worthy to note that in the absence of dust parameter, the model recover the results of Yao [15] for pure fluid flowing over the vertical wavy surface. Higher the value of dust parameter, greater will be the rate of heat transfer. As observed from the expression of α_d that dust parameter is inversely proportional to the velocity relaxation time (τ_m). Therefore, for $\tau_m >> 1$ the dust parameter will be small, i. e., $\alpha_d << 1$, on the other hand, for $\tau_m << 1$ the dust parameter must be large enough. Keeping this in mind, the numerical results displayed in Figure 6 ranges from 0.01 to 10.0. More interestingly, the waveform for $\alpha_d = 10.0$ appears very fine as compared to other disturbed waveforms, appear in the same figure.

The contribution of mass concentration parameter, $D_\rho (= 0.0, 10.0, 10000.0)$ on heat transfer rate, Q_w, is observed in Figure 7. Broken lines represent the pure fluid whereas solid lines are for dusty fluid. In the case of air/water–metal mixture; the rate of heat transfer is less in magnitude. Overall, it is revealed that the heat transfer rate diminishes owing to the increase in the mass concentration parameter D_ρ. Increment in mass concentration means that particles are loaded within the carrier phase, which as a result, reduces the temperature gradient at the wall. Therefore, it happened subject to the interaction of the two phase flow.

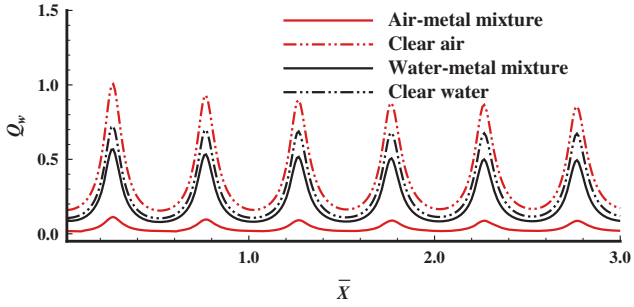

Figure 7: Local Nusselt number coefficient for air with and without particle $D_\rho = 0.0$(clear fluid), 10.0(water), 10,000.0(air) while Pr = 0.7 (air), 7.0(water), $\alpha_d = 0.5$, $\alpha = 0.5$ and $\gamma = 0.1$(water), 0.45(air).

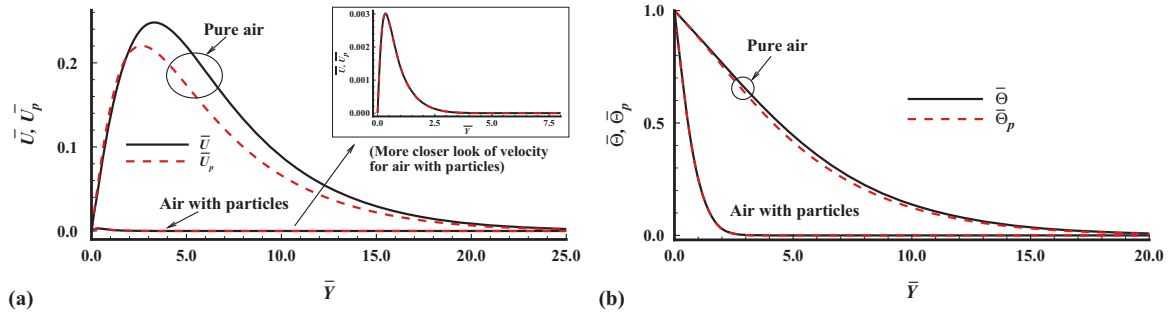

Figure 8: (a) Velocity (b) Temperature profiles for $D_\rho = 0.0, 10,000.0$, $\mathrm{Pr} = 0.7$, $\alpha_d = 0.5$, $\alpha = 0.3$, $\gamma = 0.45$ and $\bar{X} = 10.0$.

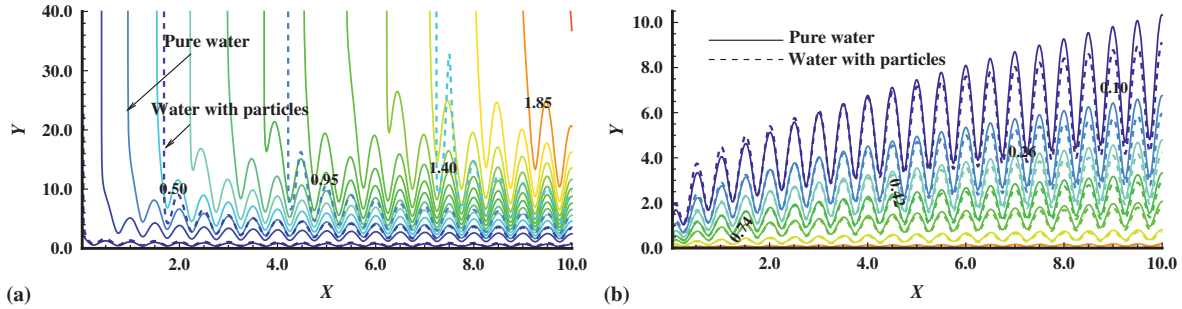

Figure 9: (a) Streamlines (b) Isotherms for $D_\rho = 0.0, 10.0$, $\mathrm{Pr} = 7.0$, $\alpha_d = 0.5$, $\alpha = 0.3$ and $\gamma = 0.1$.

The velocity and temperature distributions of the two phase problem are also important either intrinsically or because of their consequences. The velocity and temperature are schematically presented through the Figures 8 and 9. Specifically, Figure 8 display the distribution of velocity and temperature for the carrier and the particle phase for some fixed $\bar{X}$. Both profiles indicate that dusty fluid achieve asymptotic behavior very quickly as compared to pure fluid. The boxed velocity profile in Figure 8(a) gives a more closer look of fluid with dust particles and it can be concluded that particles extensively resist the flow. Moreover, in Figure 9 streamlines and isotherms are drawn. From this figure it is observed that particle cloud lies within the vicinity of the plate.

6 Conclusion

In this analysis, numerical solutions are obtained for the two phase natural convection dusty boundary layer flow, induced by the semi-infinite vertical wavy surface. Coordinate transformations (primitive variable formulations) are applied to switch the governing equations of the carrier and the dispersed phase into another set of equations. Two-point finite difference solutions are obtained for the whole length of the irregular surface. The focus of this study is to analyze the behavior of uneven surface when it is emersed in a dusty fluid. Effect of various emerging parameters are explored by expressing their relevance on the heat transfer rate. Numerical results give a clear insight towards understanding the response of the present physical situation. Velocity and temperature distributions are plotted and visualized as well through streamlines and isotherms. From this analysis, it is observed that mass concentration parameter reduces the rate of heat transfer whereas ratio of specific heat parameter, γ, enhances it considerable within the boundary layer region.

References

[1] G. Rudinger, Fundamentals of Gas-Particle Flow, Elsevier Scientific Publishing Co, New York, USA 1980.
[2] L. Farbar and M. J. Morley, Heat transfer to flowing gas-solid mixtures in a circular tube, Ind. Eng. Chem. **49** (1957), 1143–1150.
[3] F. P. Kazakevich and A. M. Krapivin, Investigations of heat transfer and aerodynamical resistance in tube assemblies when the flow of gas is dust-laden, Izv. Vissh. Uchebn. Zavedenii Energetica **1** (1958), 101–107.
[4] P. G. Saffman, On the stability of laminar flow of a dusty gas, J. Fluid Mech. **13** (1962), 120–128.

[5] C. S. Vimala, Flow of a dusty gas between two oscillating plates, Defence Sci. J. **22** (1972), 231–236.
[6] F. E. Marble. 1963. Dynamics of a gas containing small solid particles, Proceedings of the Fifth AGARD Combustion and Propulsion Colloquium, Pergamon Press, New York, 175–215.
[7] R. E. Singleton. 1964. Fluid mechanics of gas-solid particle flow in boundary layers, Ph.D. Thesis, California Institute of Technology.
[8] D. H. Michael and D. A. Miller, Plane parallel flow of a dusty gas, Mathematika **13** (1966), 97–109.
[9] D. H. Michael, The steady motion of a sphere in a dusty gas, J. Fluid Mech. **31** (1968), 175–192.
[10] N. Datta and S. K. Mishra, Boundary layer flow of a dusty fluid over a semi-infinite flat plate, Acta Mech. **42** (1982), 71–83.
[11] V. M. Agranat, Effect of pressure gradient of friction and heat transfer in a dusty boundary layer, Fluid Dyn. **23** (1988), 729–732.
[12] G. S. Roopa, B. J. Gireesha and C. S. Bagewadi, Numerical investigation of mixed convection boundary layer flow of a dusty fluid over an vertical surface with radiation, Afr. Math. **24** (2013), 487–502.
[13] S. Siddiqa, M. A. Hossain and S. C. Saha, Two-phase natural convection flow of a dusty fluid, Int. J. Numer. Method H. **25** (2015), 1542–1556.
[14] M. Molla and R. S. R. Gorla, Natural convection laminar flow with temperature dependent viscosity and thermal conductivity along a vertical wavy surface, Int. J. Fluid Mech. Res. **36** (2009), 272–288.
[15] L. S. Yao, Natural convection along a vertical wavy surface, ASME J. Heat Transfer **105** (1983), 465–468.
[16] S. G. Moulic and L. S. Yao, Natural convection along a wavy surface with uniform heat flux, ASME J. Heat Transfer **111** (1989), 1106–1108.
[17] S. G. Moulic and L. S. Yao, Mixed convection along a wavy surface, ASME J. Heat Transfer **111** (1989), 974–979.
[18] D. A. S. Rees and I. Pop, Boundary layer flow and heat transfer on a continuous wavy surface, Acta Mech **12** (1995), 149–158.
[19] D. A. S. Rees and I. Pop, Free convection induced by a vertical wavy surface with uniform heat flux in a porous medium, ASME J. Heat Transfer **117** (1995), 545–550.
[20] D. A. S. Rees and I. Pop, The effect of longitudinal surface waves on free convection from vertical surfaces in porous media, Int. Commun. Heat Mass **24** (1997), 419–425.
[21] M. A. Hossain and D. A. S. Rees, Radiation-conduction interaction on mixed convection flow along a slender vertical cylinder, J. Thermophy. Heat Transfer **12** (1998), 611–614.
[22] M. Narayana and P. Sibanda. 2011. Double diffusive convection due to a horizontal wavy surface in a porous medium, AIP Conf. Proc., 185–190.
[23] M. Narayana, P. Sibanda, S. S. Motsa and P. G. Siddheshwar. 2012. On double-diffusive convection and cross diffusion effects on a horizontal wavy surface in a porous medium, Boundary Value Problems, 2012, 88.
[24] S. Siddiqa, M. A. Hossain and C. Saha, The effect of thermal radiation on the natural convection boundary layer flow over a wavy horizontal surface, Int. J. Therm. Sci. **84** (2014), 143–150.
[25] M. M. Rashidi, A. Hosseini, I. Pop, S. Kumar and N. Freidoonimehr, Comparative numerical study of single and two-phase models of nanofluid heat transfer in wavy channel, Appl. Math. Mech. –Engl. Ed. **35** (2014), 831–848.
[26] N. Apazidis, Temperature distribution and heat transfer in a particle-fluid flow past a heated horizontal plate, Int. J. Multiphase Flow **16** (1990), 495–513.